

NAVAL POSTGRADUATE SCHOOL

Monterey, California



THESIS

MAGNETIC FIELD- INDUCED ABSORPTION OF SHORT ULTRA-INTENSE LASER PULSES

by

Kent A. Tartt

June 2000

Thesis Advisor:
Co-Advisor:

William L. Kruer
William B. Colson

Approved for public release; distribution is unlimited

DTIC QUALITY INSPECTED 4

20000911 127

REPORT DOCUMENTATION PAGE		Form Approved OMB No. 0704-0188	
Public reporting burden for this collection of information is estimated to average 1 hour per response, including the time for reviewing instruction, searching existing data sources, gathering and maintaining the data needed, and completing and reviewing the collection of information. Send comments regarding this burden estimate or any other aspect of this collection of information, including suggestions for reducing this burden, to Washington headquarters Services, Directorate for Information Operations and Reports, 1215 Jefferson Davis Highway, Suite 1204, Arlington, VA 22202-4302, and to the Office of Management and Budget, Paperwork Reduction Project (0704-0188) Washington DC 20503.			
1. AGENCY USE ONLY (Leave blank)		2. REPORT DATE June 2000	3. REPORT TYPE AND DATES COVERED Master's Thesis
4. TITLE AND SUBTITLE : Magnetic Field-Induced Absorption of Short Ultra-Intense Laser Pulses		5. FUNDING NUMBERS	
6. AUTHOR(S) Tartt, Kent A.			
7. PERFORMING ORGANIZATION NAME(S) AND ADDRESS(ES) Naval Postgraduate School Monterey, CA 93943-5000		8. PERFORMING ORGANIZATION REPORT NUMBER	
9. SPONSORING / MONITORING AGENCY NAME(S) AND ADDRESS(ES) N/A		10. SPONSORING / MONITORING AGENCY REPORT NUMBER	
11. SUPPLEMENTARY NOTES The views expressed in this thesis are those of the author and do not reflect the official policy or position of the Department of Defense or the U.S. Government.			
12a. DISTRIBUTION / AVAILABILITY STATEMENT Approved for public release; distribution is unlimited		12b. DISTRIBUTION CODE	
13. ABSTRACT (maximum 200 words) Self-generated magnetic fields up to 10^9 Gauss have been predicted in plasmas irradiated with ultra-intense laser light pulses with overdense plasmas. We find that the laser absorption can be significantly enhanced by the oscillation of electrons across these fields. There is then a very large Lorentz force, which can strongly accelerate electrons into the plasma and can lead to generation of harmonics in the reflected light. We also show that large magnetic fields can be significantly amplified to even larger values by the pressure of the light pulse. Potential applications are discussed.			
14. SUBJECT TERMS Ultra-Intense Laser Pulses, Computer Simulations, Magnetic Fields			15. NUMBER OF PAGES 54
			16. PRICE CODE
17. SECURITY CLASSIFICATION OF REPORT Unclassified	18. SECURITY CLASSIFICATION OF THIS PAGE Unclassified	19. SECURITY CLASSIFICATION OF ABSTRACT Unclassified	20. LIMITATION OF ABSTRACT UL

THIS PAGE INTENTIONALLY LEFT BLANK

Approved for public release; distribution is unlimited

**MAGNETIC FIELD-INDUCED ABSORPTION OF SHORT
ULTRA-INTENSE LASER PULSES**

Kent A. Tartt
Lieutenant Commander, United States Navy
B.S., Yale University, 1985

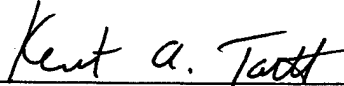
Submitted in partial fulfillment of the
requirements for the degree of

MASTER OF ARTS SCIENCE IN APPLIED PHYSICS

from the

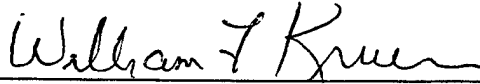
**NAVAL POSTGRADUATE SCHOOL
June 2000**

Author:

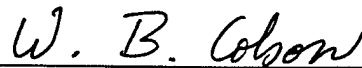


Kent A. Tartt

Approved by:



William L. Kruer, Thesis Advisor



William B. Colson, Co-Advisor



FOR William Maier, Chairman
Department of Physics

THIS PAGE INTENTIONALLY LEFT BLANK

ABSTRACT

In order for the NIF (National Ignition Facility) to achieve its most challenging goal of fusion, it is paramount that we explore new laser matter interaction regimes and control mechanisms. This thesis explores a novel interaction regime namely, the enhancement of laser absorption when an overdense plasma is irradiated with ultra-intense laser light. Self-generated magnetic fields of up to 10^9 gauss have been predicted in overdense plasmas irradiated with ultra-intense laser light pulses. We find that laser light absorption can be significantly enhanced by the oscillation of electrons across these fields. There is then a very large Lorentz force, which can strongly accelerate electrons into the plasma and can lead to generation of harmonics in the reflected light. We also show that large magnetic fields can be significantly amplified to even larger values by the pressure of the light pulse. Potential applications of this interaction regime include the Fast Igniter approach to ICF (Inertial Confinement Fusion), the creation of anti-matter, and the development of laser radiography to name a few. Zohar, a 2- $\frac{1}{2}$ D PIC (Particle In Cell) code was used to run our simulations. Zohar assumes a collisionless plasma, solves Maxwell's equations in 3D, and accounts for the relativistic effects which can occur in the high-energy regime that we consider. The high number of particles simulated required significant computing power, which was obtained by remote access to the LC (Livermore Computing) East computer, which provided 8 processors and 8 GB of shared memory at 440 MHz. "Exceed" software was required to graphically display our results on a PC. This thesis has been a collaborative effort between NPS (Naval Postgraduate School) and LLNL (Lawrence Livermore National Laboratories), to the benefit of DoD.

THIS PAGE INTENTIONALLY LEFT BLANK

TABLE OF CONTENTS

I. INTRODUCTION	1
A. BASIC PLASMA CONCEPTS	1
1. Concept of Temperature	2
2. Plasma Instabilities	4
3. Self Generated Magnetic Fields in Plasmas	5
B. COMPUTER SIMULATION OF PLASMA USING PARTICLE CODES	6
1. Basic Ingredients of a Particle Code	8
2. PIC Code Programming Considerations	11
II. ULTRA-INTENSE REGIME OF LASER MATTER INTERACTIONS	15
A. SIMPLE MODELS FOR REALISTIC LASERS AND SOLIDS	18
III. EFFECT OF LARGE SELF-GENERATED MAGNETIC FIELDS ON ULTRA INTENSE LASER PLASMA INTERACTIONS	23
IV. CONCLUSION	35
LIST OF REFERENCES	39
INITIAL DISTRIBUTION	41

The author extends special thanks to the following individuals for aiding in this project to its completion:

- To the Chairman of the Physics Department at NPS, Professor William Maier and my Curriculum Advisor (Code 34) Commander T. Mc Coy for allowing me to attend the 41st Annual DPP (Division of Plasma Physics) conference, and the 30th Anomalous Absorption conference. These forums provided an invaluable opportunity to catch a glimpse of state of the art research in Plasma Physics.
- To My Thesis Advisor, Professor William Kruer, who along with being a great professor has been a mentor and dear friend. His inspiring lectures have given me special appreciation for the words of one of his favorite great thinkers,

“The search for truth is in one way hard and in another way easy, for it is evident that no one can master it fully or miss it wholly. But each adds a little to our knowledge of nature, and from all the facts assembled there arises a certain grandeur”.- Aristotle

It has been an a unique privilege to have been a student of a brilliant scientist and teacher who is so prolific in the advancement Plasma Physics research. I am forever indebted.

- To Dr. Scott C. Wilks at Lawrence Livermore Labs for his indispensable assistance in the execution and interpretation of the complex computer simulations and programming algorithms. Dr. Wilks, your insight in Plasma Physics combined with your computer skills are truly impressive!
- Dr. Hector Boldes and Mrs. Mary Ann Soby of the Institute for Laser Science and Applications for their hospitality in providing an office and computer at Lawrence Livermore labs.
- Most importantly, may I offer thanks to God for blessing me with the opportunity to attend the Naval Postgraduate School, which has been the fulfillment of a dream after 15 years of Naval service.

I. INTRODUCTION

The study of the interaction of intense laser light with plasmas serves as an excellent introduction to the field of plasma physics [Ref. 1]. Both the linear and nonlinear theories of plasma waves, instabilities and wave-particle interactions are important for understanding laser plasma coupling. Numerous plasma effects have been observed in laser plasma experiments, and many challenging problems remain to be understood.

A. BASIC PLASMA CONCEPTS

Plasma is a medium containing many charged particles governed by electromagnetic forces. Plasma is a quasineutral gas of charged particles, which possess collective behavior. Plasma designates the fourth state of matter, which exists in the sun, stars, and space, etc; moreover, most of the Universe is made up of plasma. The plasma medium is described macroscopically (on a large scale) by its temperature and density, and changes in the plasma are calculated by using conservation equations such as conservation of energy, momentum and mass. On a microscopic (small) scale, a statistical description using probabilities is required to describe a plasma in the calculation of the positions and velocities of all particles. Due to their mutual collisions, the plasma charged particles emit radiation (electromagnetic waves). Moreover, many different waves can be created in a plasma medium. The stabilities and instabilities of these waves play a crucial role in plasma systems. Plasma plays an important role in explaining our universe and, as we shall see, scientists believe that the understanding of plasma is the key issue for solving the energy problems of mankind.

A plasma is basically a system of N charges that are coupled to one another via their self-consistent electric and magnetic fields. Following the evolution of these N charges in principal would require us to solve $6*N$ coupled equations which would be tedious at best. Fortunately, great simplification is possible if we focus our attention on the collisionless plasma behavior.

Let us assume a plasma space in which we decompose the electric field into two fields (E_1 and E_2) that have distinct spatial scales. The field E_1 has spatial variations on a scale length much less than the electron Debye length λ_{De} . The field of an individual charge is shielded out by the response of the surrounding charges over this length. E_1 represents the rapidly fluctuating microfield due to multiple and random encounters (collisions) among the discrete charges. In contrast, the field E_2 varies on a space scale greater than or comparable to λ_{De} . E_2 represents the forces due to the average or “collective” motion of the charges.

We thus have a natural separation into collisional and collective behavior. The collisional behavior becomes negligible when the number of electrons in the sphere with a radius equal to the electron Debye length becomes very large.

1. Concept of Temperature

In order to better understand the complex nature of plasma behavior, it is necessary to expand our most basic notion of temperature [Ref. 2]. We note that a gas in thermal equilibrium has particles of many different velocities and the most probable distribution of these velocities is known as the Maxwellian distribution. The average kinetic energy (E_{ave}) in three dimensions is:

$$E_{ave} = 3/2 KT \tag{1}$$

where K is Boltzmann's constant, $K = 1.38 \times 10^{-23} \text{ J/}^\circ\text{K}$ and T is the temperature in degrees Kelvin. The general result here is that E_{ave} is $\frac{1}{2} KT$ per degree of freedom. It is customary in plasma physics to give temperatures in units of energy. To avoid confusion on the number of dimensions involved, it is not E_{ave} but the energy corresponding to KT that is used to denote the temperature. For $KT = 1 \text{ eV} = 1.6 \times 10^{-19} \text{ J}$, we have $T = 1.6 \times 10^{-19} / 1.38 \times 10^{-23} = 11,600$, thus the conversion factor is $1 \text{ eV} = 11,600^\circ \text{ K}$.

It is interesting that plasma can have several temperatures at the same time. It often happens that the ions and electrons have separate Maxwellian distributions with different T_i and T_e (ion and electron temperatures respectively). This comes about because the energy exchange between colliding electrons is larger than that between an ion and electron. Since colliding electrons are the same size and mass, appreciable kinetic energy exchanges can result from an electron-electron collision. Now, when an electron-ion collision occurs, we recall that the electron is only $1/3700^{\text{th}}$ the mass of an ion and therefore a finite amount of time (on the order of hundreds of microseconds let's say) is required for a couple thousand electrons to collide with an individual ion to result in an appreciable kinetic energy exchange. Bearing this in mind, we can see how each species can be in its own thermal equilibrium but the plasma may not last long enough for the two temperatures to equalize (since many of the interesting effects of the experiments are observed in nanoseconds).

When there is a magnetic field B , even a single species, say ions, can have two temperatures. This is because the forces acting on ions along B are different from those acting perpendicular to B (due to the Lorentz force). The components of velocity

perpendicular to B and parallel to B may then belong to different Maxwellian distributions with temperatures T_{parallel} and $T_{\text{perpendicular}}$.

Interestingly enough, a high temperature does not necessarily mean a lot of heat [Ref. 2]. For example, the electron temperature inside a fluorescent light bulb is about 20,000° K, but it is cool to the touch. This is because heat capacity has to be considered. The heat capacity of the electrons in the fluorescent light bulb is minimal because the electron density is much less than that of a gas at atmospheric pressure and the amount of heat transferred to the wall by electrons striking it at their thermal velocities is minimal.

2. Plasma Instabilities

Plasmas behave in a collective way. Different types of waves are created in the plasma due to the collective behavior of the electrons and the ions [Ref. 2]. The types of waves that can be created in plasma are numerous and we shall mention just a few of the most fundamental ones to the study of plasma behavior.

Conditions of collective motion can be stable or unstable. For example, suppose a small displacement takes place in plasma confined by a magnetic field. If the collective motion behaves in a stable way, the displacement will be restored to the original motion. However, if the collective motion is unstable, any small displacement increases rapidly resulting in the collective motion phenomenon breaking up.

Numerous instabilities can be excited by an intense electromagnetic wave in a plasma. Many possibilities exist even without dc magnetic fields [Ref. 1]. These various instabilities can be thought of as the resonant coupling into two other waves. Various possibilities and their names are shown below.

- Ion acoustic decay instability $\omega_0 \rightarrow \omega_{pe} + \omega_i$ at $n \cong n_{cr}$

- Raman instability $\omega_0 \rightarrow \omega_{sc} + \omega_{pe}$ at $n \leq 1/4 n_{cr}$
- Brillouin instability $\omega_0 \rightarrow \omega_{sc} + \omega_i$ at $n \leq n_{cr}$
- $2 \omega_{pe}$ instability $\omega_0 \rightarrow \omega_{pe} + \omega_{pe}$ at $n \cong 1/4 n_{cr}$

Here, ω_0 is the incident light frequency, ω_{sc} is the frequency of a scattered light wave ω_{pe} is the frequency of a high frequency electron plasma wave, ω_i is the so-called ion sound frequency and n_{cr} is the critical density in the plasma at which an incident light wave is reflected.

3. Self Generated Magnetic Fields in Plasmas

Experiments and calculations have shown the existence of self-generated magnetic fields [Ref. 3]. These magnetic fields can be generated in many different ways [Ref. 4]. Let's consider the simplest way. Consider a target irradiated by high intensity laser light. There will be both a density and temperature gradient in the resulting plasma, as indicated in Figure 1. When the cross product between the density gradient (∇n) and the temperature gradient (∇T) is nonzero, a magnetic field is generated. Faraday's law shows that \dot{B} is nonzero (i.e., a magnetic field grows up) whenever there is a curl of the electric field. In an expanding plasma, the electric field is proportional to the gradient of the pressure (∇nKT) divided by the density. One then finds that a magnetic field is generated whenever $\nabla n \times \nabla T \neq 0$.

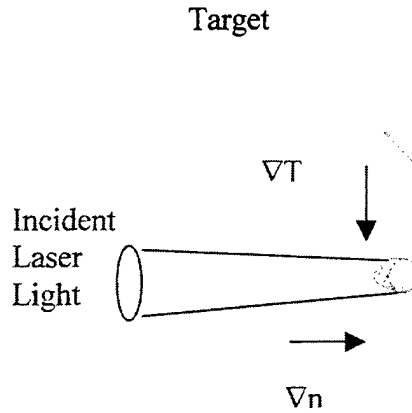


Figure 1. A schematic illustrating crossed density and temperature gradients generated when a target is irradiated.

B. COMPUTER SIMULATION OF PLASMA USING PARTICLE CODES

A theoretical description is often used where the plasma is treated as two charged fluids. We will use a complementary numerical description of plasma behavior using particle codes [Ref. 1,5,6]. Computer simulation of plasma using particle codes is a very direct and powerful approach, particularly for investigating kinetic and/or nonlinear effects. Since we are investigating strongly nonlinear plasma effects, we utilize the power of the computer to simulate the behavior of the charged particles of plasma. The approach is as follows: numerically follow the motion of a large collection of charges in their self-consistent electric and magnetic fields. The basic cycle is illustrated in Figure (2).

From the positions and velocities at any given time, we compute the charge and current densities on a spatial grid that is fine enough to resolve the collective behavior of the charges. Using the computed charge and current densities, then compute the self-consistent electric and magnetic fields via Maxwell's equations. Next, we use these

fields in the equations of motion to advance the positions and velocities of the charges. Finally, continue around this basic cycle with a time step sufficiently small to resolve the highest frequency in the problem (which is often the electron plasma frequency ω_{pe}).

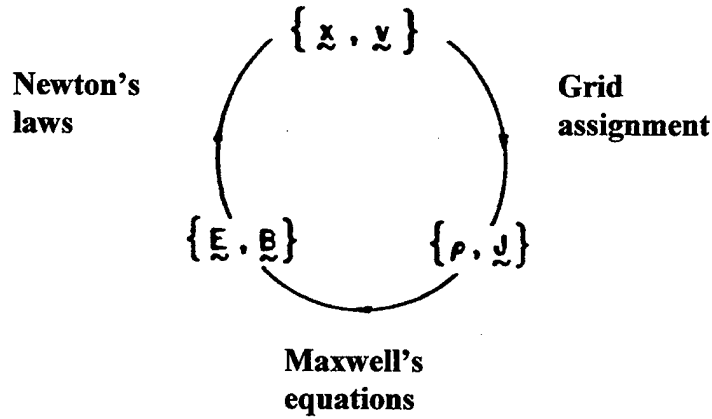


Figure 2. The Basic Cycle of a Particle Simulation Code, From Ref.[1].

While plasma actually consists of a huge number of particles, particle simulations are limited by the capabilities of computers to 10^4 to 10^8 particles, and a single simulation particle must therefore represent a large number of actual particles. Since we seek to describe the collective behavior of the plasma, we can follow behavior on characteristic length ℓ , which is larger than the Debye length λ_{De} , to simplify our analysis and not consider the fine-scale fluctuating microfields associated with particle discreteness. This simplification allows us to represent the fields on a discrete grid in space, which is fine enough to resolve the collective behavior and sufficiently coarse to ignore the microfields. A mesh size $\delta \approx \lambda_{De}$ is usually chosen.

Alternatively, this spatial averaging process can be viewed as using “finite-size” particles of size $\delta \approx \lambda_{De}$. The behavior of a group of such particles is the same (with

minor modifications) as the behavior of point charges for scale lengths $\ell \gg \delta$, but fluctuations with scale lengths $\ell \ll \delta$ are suppressed. Hence, we achieve with a “trick” what nature does with the use of an enormous number of particles; i.e., smooth over the fine scale length microfields.

1. Basic Ingredients of a Particle Code

All particle codes share some basic ingredients, which we shall illustrate. We treat the ions as a fixed, neutralizing background, assume no imposed magnetic fields, and consider only electrostatic fields. In this electrostatic limit, the magnetic field generated by plasma currents is negligible, and Maxwell’s equations reduce to Poisson’s equation, which for simplicity we look at in only one dimension:

$$\epsilon_0 \nabla^2 \phi = \epsilon_0 \partial^2 \phi / \partial x^2 = -e(n_i - n_e) \quad (2)$$

In this equation, ϵ_0 is the permittivity constant of free space, ϕ is the electric field potential, e is the electron charge, n_e and n_i being the electron and ion charge densities respectively. Variations are allowed in only one direction, and periodic boundary conditions are adopted.

Our first task is to compute the charge density. Our system extends from 0 to L , as shown in Figure (3). We divide this system into NC cells and for convenience take the cell size (δ) to be unity (i.e., $L = NC$). The grid points are identified as the integer values of the position, augmented by one so that the counting begins with one. Note that the $(NC + 1)^{\text{th}}$ grid point is then identical with the first, due to the assumed periodic boundary conditions. Given the position of the charge, many schemes can be used to assign it to the spatial grid. For example, we could just assign the charge to its nearest grid point

location. A better scheme is to share the charge between its two nearest grid points. (see Figure 3)

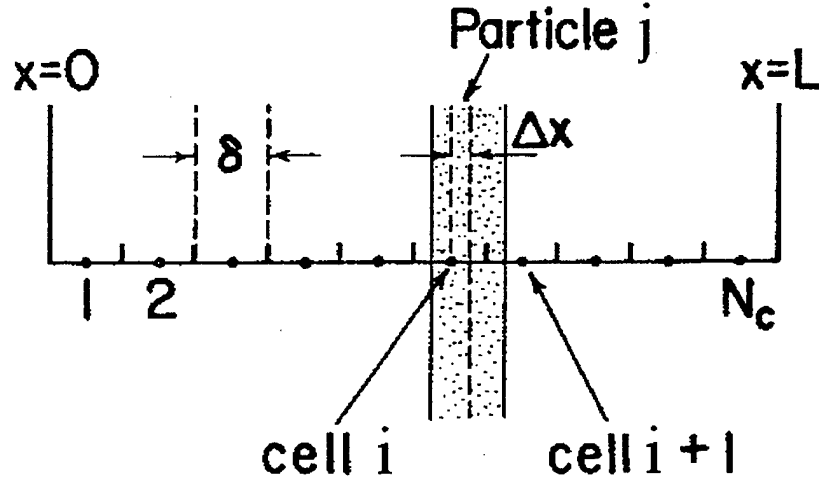


Figure 3. The charge-sharing scheme for finite sized particles, From Ref.[1].

For a charge located a distance Δx to the right of the i^{th} grid point, we then have:

$$\Delta\rho(i) = q(1 - \Delta x) \quad (3)$$

$$\Delta\rho(i+1) = q \Delta x ,$$

where $\Delta\rho$ is the increment to the charge density.

Having assigned the charges and determined the charge density on the spatial grid, we next determine the self-consistent electric field using Poisson's equation

$$\partial E / \partial x = \rho / \epsilon_0 \quad (4)$$

The simplest approach is to finite-difference Poisson's equation,

$$E(i+1) = E(i) + \delta [(\rho(i+1) + \rho(i))/2] (1/\epsilon_0) \quad (5)$$

An alternative approach is to Fourier transform the charge density, use Poisson's equation to find $E_k (ikE_k = \rho_k/\epsilon)$, and invert the transform to determine the electric field on the spatial grid.

The last step in the basic cycle is to use the electric field to move the particles. The electrical force is assigned from the grid to the individual particles using the same scheme chosen to assign the charges to the grid. For example, considering a particle a distance Δx to the right of the i^{th} grid point and using linear interpolation, we obtain for the force F on the particle

$$F = qE(i)[1 - \Delta x] + qE(i+1)\Delta x \quad (6)$$

In this code, Poisson's equations are only solved for the electric field and the magnetic field is assumed zero. Therefore, the velocity (v) and position (x) of each particle can be advanced Δt in time using a "leap frog" algorithm; i.e.,

$$v^{n+1/2} = v^{n-1/2} + F^n \Delta t \quad (7)$$

$$x^{n+1} = x^n + v^{n+1/2} \Delta t \quad (8)$$

The superscripts denote time step. By defining x and v one-half time step apart, we achieve second-order accuracy in the time step. In the initial conditions, x and v are defined at the same time ($t=0$), but it is straightforward to then displace the velocities backward in time using the force at $t=0$.

The plasma evolution is computed by simply continuing around the basic cycle using a time step small enough to resolve the characteristic oscillations of the plasma. In this electrostatic limit, the highest frequency oscillation has a frequency near ω_{pe} , the electron plasma frequency. Hence, a time step of about $0.2\omega_{pe}^{-1}$ is commonly used

Of course, it is also necessary to resolve the scale lengths characteristic of the collective behavior. Hence a grid size of about λ_{de} is commonly used. It is interesting to note that a numerical instability would be introduced if the grid size were chosen to be too many λ_{de} . This instability is due to aliasing, which arises from the fact that on the grid a disturbance with wave number k cannot be distinguished from spurious ones with wave numbers $k + 2\pi n/\delta$ where δ is the grid spacing and n is an integer [Ref. 1,19].

2. PIC Code Programming Considerations

Random particle initialization is the simplest and most commonly used method. However, it introduces noise in the computations which can mask interesting physical phenomena, particularly when we wish to study the low amplitude linear regime. In such cases the programs utilize what is referred to as a “quiet start” which avoids this background noise introduced by the randomness of the numbers. The program that simulates the plasma particle behavior can remain in this “quiet” state for only a finite time, which must be long enough to allow observation of the low-amplitude phenomena being studied. In such cases, staggering the particles, so that they do not form exact beams, is an effective way to delay the onset of the noisy behavior.

Even with this simplest of particle code, many instructive and interesting plasma problems can be examined. As one example, let's use ES1, a flexible and optimized 1d electrostatic PIC code to look at the strongly non-linear behavior of a two-stream instability [Ref. 5].

In this simple case, half the electrons are given an initial drift velocity in one direction and half in the other direction. This counter streaming motion is a source of free energy, which drives unstable a variation in density and potential.

Figure 4a shows the electron phase space (velocity versus position for all the electrons), electric field and the potential at an early time. Note the counter streaming plasmas. In Figures 4b and Figure 4c, the effect of the instability on the electric field and the potential in the plasma can be seen. Finally, the growing electric field becomes so large that vortices form in phase space, as the electrons are alternatively slowed down and speeded by the large electric field, as shown in Figure 4c. Figure 4d shows time histories of the kinetic energy, the electric field energy and the total energy of the system. Note the exponential growth of the electric field energy at early times and the subsequent saturation. As the electric field energy increases, the kinetic energy decreases. The total energy varies very little compared to these changes, showing that the code is conserving energy with sufficient accuracy.

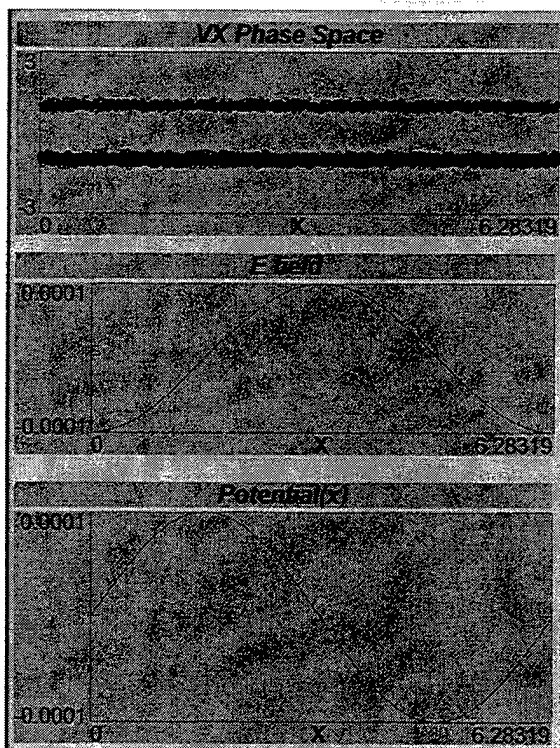


Figure 4a

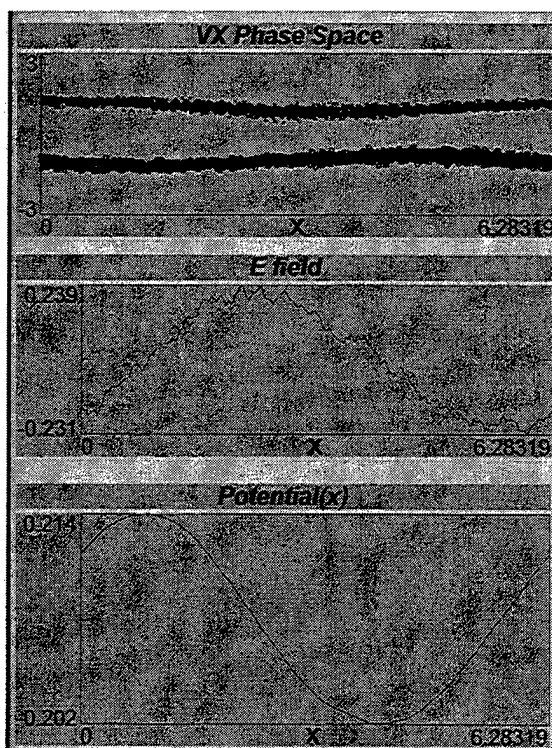


Figure 4b

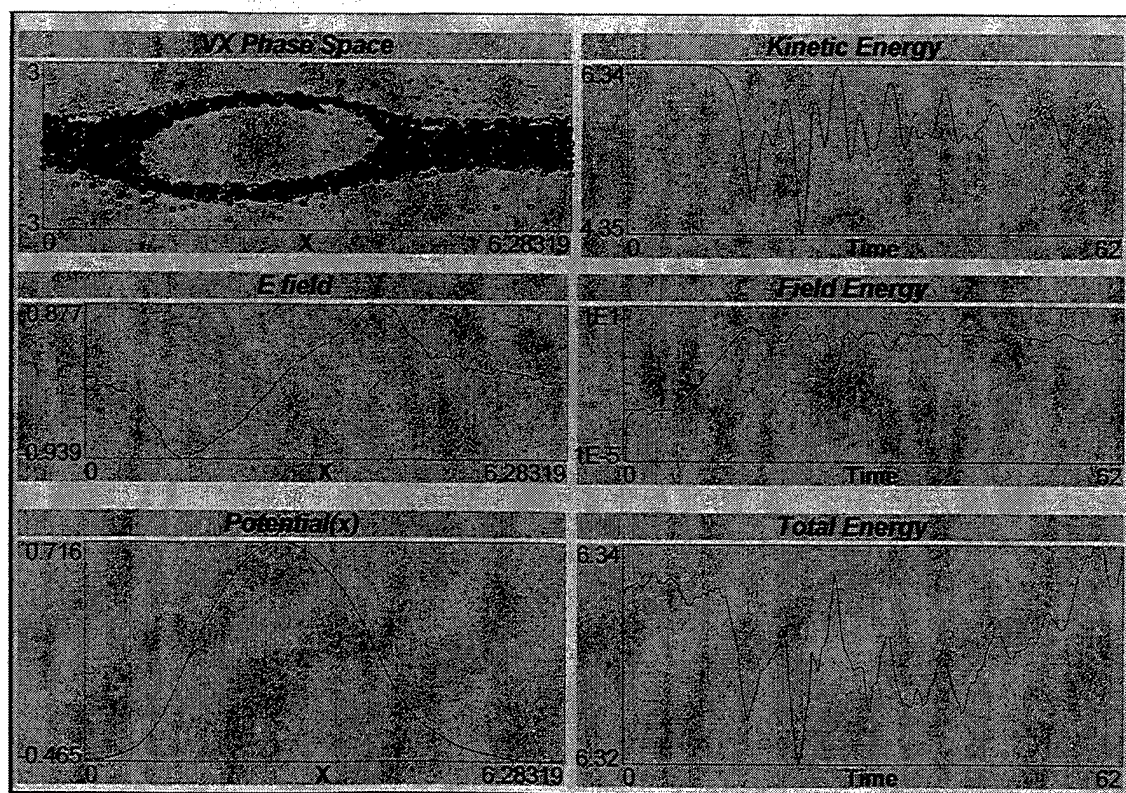


Figure 4c

Figure 4d

Figures 4a-c show V_x Phase Space , Electric Field, and Potential respectively versus x . Figure 4 d shows Kinetic, Electric Field, and Total energies respectively versus time.

Zohar represents a significant improvement to ES1 in PIC modeling of plasma behavior. This code solves all of Maxwell's equations in order to include light waves and uses equations of motion that are relativistically correct. Zohar (which means brilliance or radiance in Hebrew) is the 2 ½ D PIC code used at Lawrence Livermore Labs to model the interaction of intense laser light with plasmas and for some electron beam-plasma studies[Ref. 7]. 2 ½ D means that variations are followed in two directions, and that all three velocities are included in the code calculations. We note that state of the art, three-dimensional PIC codes, which run on parallel machines, now exist [Ref. 8,9]. The simulations that follow are results of Zohar runs.

II. ULTRA-INTENSE REGIME OF LASER MATTER INTERACTIONS

The recent development of Ultra Short Ultra-Intense (US-UI) laser pulses has allowed for the generation of laser intensities that are orders of magnitude over what was possible with previous laser technology [Ref.10]. The ultrashort regime includes laser light with pulse lengths τ_p of about 10 femtoseconds (fs) up to 10 picoseconds (ps). The ultra-intense regime covers intensities starting at about 10^{17} W/cm². The ultra-intense regime is usually defined as the point at which the normalized amplitude of the electric field of the laser light is greater than or equal to 1, i.e., $eE_o/m_e\omega_o c \geq 1$ [Ref.11]. Here, E_o is the electric field amplitude of the laser light, m_e is electron rest mass, ω_o is the frequency of the laser light, and c is light speed. Even as late as ten years ago, most lasers could not produce light that could approach this electric field strength, with the exception of a few CO₂ lasers built in the 1970's. Now, there are a large number of ultra-intense lasers all over the world. What made this possible was the application of chirped pulse amplification (CPA) [Ref. 10], originally developed in microwave technology, to laser systems. This breakthrough in laser hardware has spawned considerable interest in US-UI laser-matter interactions. Never before has it been possible to deposit so much laser energy in such a short amount of time, in such a tiny volume on the front of a solid target.

Chirped Pulse Amplification is critical because laser pulses of extremely high power density (gigawatts/centimeter²) can severely damage optical components such as amplifiers, lenses, and mirrors. CPA technology allows very short laser pulses to generate extremely high peak powers by stretching the initially low-energy laser pulse

more than 10,000 times its duration before amplifying it and recompressing the pulse back to near the original duration after amplification. Damage to the laser optics is avoided by passing the long low power pulse through the amplifier (see Figure 5).

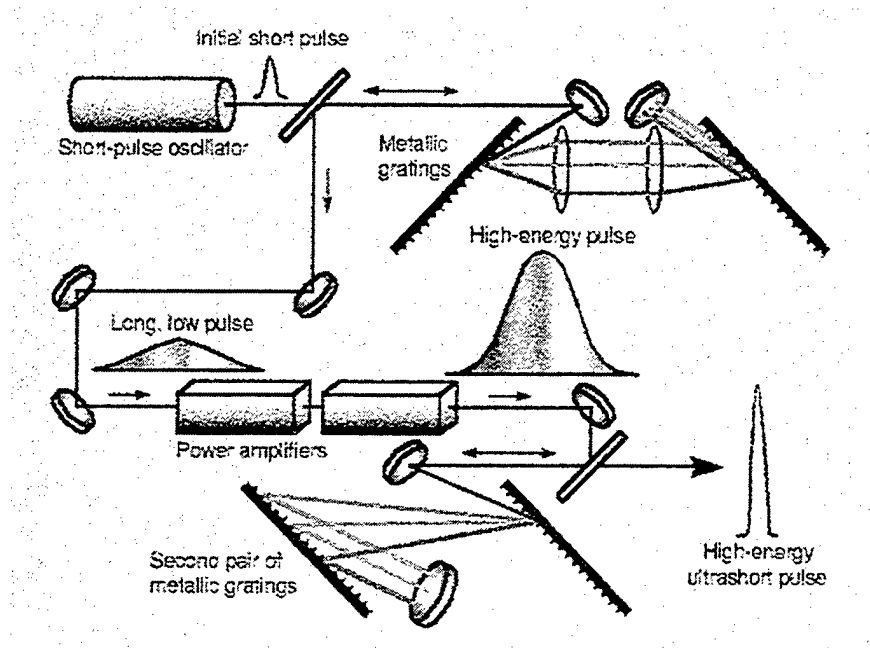


Figure 5. The concept of chirped-pulse amplification and other new technologies enabling the production of ultra-intense pulses, From Ref.[10].

Previously, the intense CO₂ lasers were nanoseconds long, which creates large preformed plasmas that the laser interacted with. There was then a considerable amount of absorption in the underdense part of the plasma, as well as enough time for the laser to filament on its way to the critical surface. This, in turn, led to a large fraction (> 10%) of the laser energy converted to hot electrons, which were thought to be created by various laser-plasma interactions. However, US-UI laser pulses can have pulse lengths of the order of picoseconds and shorter. This means that they have the ability to both create a

dense plasma (sometimes several times the critical density and up to solid densities) and interact with it, if proper care is taken to eliminate the pre-pulse.

The interaction of an intense laser with very dense plasma is interesting for several reasons. First, since the laser light is absorbed most efficiently near the critical surface, the material can potentially absorb a large fraction of the laser light. Laser light transfers energy to the plasma via the electrons. Electrons readily oscillate in the electric field of the laser. This motion is referred to as the quiver velocity, and is defined as

$$p_{osc}/m_e c = \gamma v_{osc}/c = eE_0/m_e c \omega_0 = \sqrt{I \lambda_\mu^2 / 1.3 \times 10^{18}} \quad (9)$$

Here, p_{osc} (v_{osc}) is the transverse quiver momentum (velocity) of an electron in the laser field with an electric field amplitude of E_0 , I the laser intensity (in W/cm^2), λ_μ is the laser wavelength in microns, and γ is the relativistic factor defined below. The energy associated with this momentum can easily reach MeV levels for electrons in the presence of lasers with (normalized) intensities $10^{19} \text{ W} \cdot \mu\text{m}^2/\text{cm}^2$. Therefore, relativistic effects become important for these interactions, and are included in calculations concerning US-UI laser-matter interactions. Note that the quiver velocity scales in terms of $I \lambda^2$. This is a common scaling, and so it is useful to introduce this as the normalized intensity. In this way, many results discussed can easily be applied to any wavelength laser desired.

A. SIMPLE MODELS FOR REALISTIC LASERS AND SOLIDS

An ideal model for ultra-intense pulses interacting with solids would require that a perfect Gaussian laser pulse, with a temporal pulse length (FWHM) of τ_0 and a peak intensity of I_0 , strike a solid with a step-like density interface [Ref.11]. When the laser intensity exceeds about 10^{12} W/cm², ionization of the electrons in the target occurs, and a plasma is formed on the surface of the solid. Typical ion densities are $n_i \approx 10^{23}$ cm⁻³, and electron densities are $n_e = Z n_i$. For US-UI pulses, this happens quite early in the interaction, and so most of the pulse interacts with a plasma, as opposed to an un-ionized solid. The relativistically correct dispersion relation (for circular polarization) that governs the propagation of light waves in the plasma is given by

$$kc = \sqrt{\omega_{pe}^2 / \gamma - \omega_0^2} \quad (10)$$

where $k(\omega_0)$ is the wavenumber (frequency) of the laser light,

$$\gamma = \sqrt{1 + p_{osc}^2 / (m_0 c)^2} \quad (11)$$

is the relativistic factor, and

$$\omega_{pe} = \sqrt{4\pi n_e e^2 / m_e} \quad (12)$$

is the plasma frequency.

First, consider the nonrelativistic case where $\gamma \approx 1$, which is valid up to (normalized) intensities of about 5×10^{17} W·μm²/cm². In this case, k approaches zero when $\omega_{pe} = \gamma \omega_0$. The laser no longer propagates, but is reflected when this condition is satisfied. The density at which this occurs is called the critical density and is given by

$$n_{cr} = \gamma 1.1 \times 10^{21} / \lambda_\mu \text{ cm}^{-3} \quad (13)$$

where λ_μ is the laser wavelength in micrometers. The laser light does penetrate slightly past critical, but falls off exponentially in a distance determined by the plasma density. This distance is known as the collisionless skin depth and is given by c/ω_{pe} in the nonrelativistic limit. For example, for a solid target of carbon ($Z = 6$), the skin depth is about 6 nm (nanometer = 10^{-9} m).

For the relativistic case ($\gamma > 1$), we see that the effective density at which the light will be reflected from the plasma has increased by the factor γ . Thus, in the relativistic case laser light can propagate even further into the overdense plasma due to the mass of the electrons increasing as they become relativistic. This increase in inertia makes it more difficult to generate the oscillating current in the plasma needed to reflect the laser light.

A second interesting effect evident in US-UI laser matter interactions is that the laser pressure can easily be larger than the plasma pressure, even for extremely dense plasmas. The pressure associated with a laser with intensity I (in W/cm^2) is

$$p_L = 330I/10^{18} \text{ Mbar} \quad (14)$$

Efficient coupling of laser light to electrons has been exploited in two ways to date. First, there has been considerable effort at trying to use these interactions to produce high brightness X-ray lasers [Ref. 11]. Second, the possibility of generating large numbers of energetic electrons has been proposed as a novel way to deliver a large amount of energy to a hot spot in a compressed core of deuterium and tritium in order to ignite a fusion pellet. This is commonly known as the Fast Igniter fusion scheme [Ref. 12]. Central to both of these applications is the question of efficiency. How efficient is the coupling of laser light to the production of hot electrons? How does it

scale with laser intensity, wavelength, f-number, or spot size? How does the efficiency scale with the plasma parameters such as temperature, density, and scale length? [Ref.13]

Computer simulations using Particle-In-Cell codes were used to provide an early glimpse into the ultra-intense regime. As a simple example, consider a two-dimensional simulation of a focused light beam with intensity $I\lambda_{\mu}^2 = 10^{19} W \cdot \mu m^2 / cm^2$ incident onto an overdense plasma. Over a third of the light was found to be absorbed into very energetic electrons as shown by Figure 6a [Ref. 13]. These electrons had an effective temperature of about 1 MeV at this intensity. As shown in Figure 6b, the light pressure punched a hole in the plasma, causing it to recede at a significant fraction of the velocity of light. Both of these effects have now been observed. Very large self-generated magnetic fields were found in these simulations (up to 10^9 Gauss!).

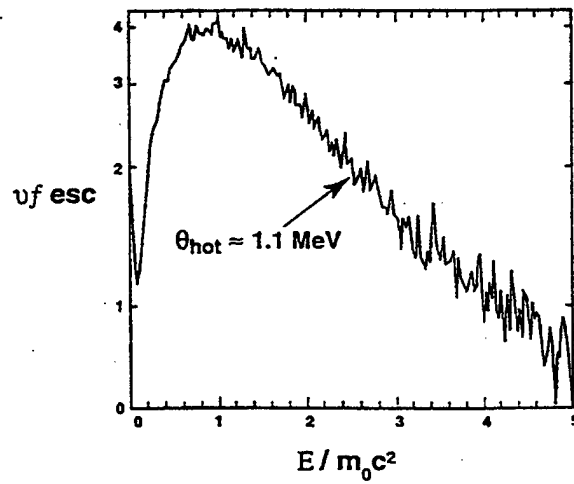


Figure 6a, From Ref.[13]. A plot of the energy distribution of escaping electrons.

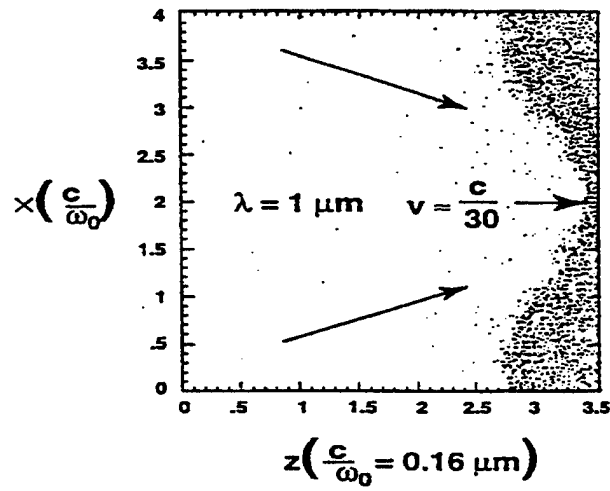


Figure 6b, From Ref.[13]. A plot of electrons in space showing a hole being punched into the plasma.

THIS PAGE INTENTIONALLY LEFT BLANK

III. EFFECT OF LARGE SELF-GENERATED MAGNETIC FIELDS ON ULTRA INTENSE LASER PLASMA INTERACTIONS

The focus of this thesis is to show how large self-generated magnetic fields affect the interaction of ultra-intense laser pulses with plasmas as found in the early simulation studies just discussed, the magnitude of the self-generated magnetic (B_{dc}) field can be estimated as $B_{os}/3$, where B_{os} is the amplitude of the oscillating magnetic field of the short, intense laser pulse. In other words, about 10% of the energy of the oscillating magnetic field was “rectified”. When targets are irradiated with $1.06\mu\text{m}$ laser light with intensities ranging from 10^{18} W/cm^2 to 10^{21} W/cm^2 , B_{dc} can become very large, with typical values of 30-900 MG as shown in Table I. To put such large magnetic fields into perspective, we note the following:

- The approximate magnetic field at the earth's surface
 $\approx 10^{-4} \text{ T} \approx 1 \text{ Gauss}$.
- The approximate magnetic field near a big electromagnet
 $\approx 1.5 \text{ T} \approx 1.5 \times 10^4 \text{ Gauss}$.
- The approximate magnetic field near the surface of a neutron star
 $\approx 10^8 \text{ T} \approx 10^{12} \text{ Gauss}$ [Ref.14].

$I(\text{W/cm}^2)$	$B_{dc}(\text{MG})$	γ	ω_{ce}/ω_0
10^{18}	30	1.2	0.7
10^{19}	90	2.1	0.4
10^{20}	300	6.1	0.5
10^{21}	900	19	0.5

Table 1. Typical estimated values of B_{dc} and cyclotron frequency in the ultra-intense laser regime. Here $\omega_{ce} = eB_{dc}/mc\gamma$ and $\gamma = (1 + I\lambda_\mu^2/2.8 \times 10^{18})^{0.5}$

Some other characteristic parameters are also shown in Table I. The electron motion in such intense laser light can become relativistic. The relativistic factor γ is estimated as:

$$\gamma = (1 + I\lambda_\mu^2/2.8 \times 10^{18})^{1/2}, \quad (15)$$

where linearly polarized light has been taken. Typical values of γ range from 1.2 to 19.

The characteristic frequency with which electrons gyrate (see Figure 7) about the magnetic field is the so-called electron cyclotron frequency ω_{ce} , where

$$\omega_{ce} = eB_{dc}/m\gamma \quad (16)$$

As shown, ω_{ce} becomes a significant fraction of ω_0 , the laser light frequency.

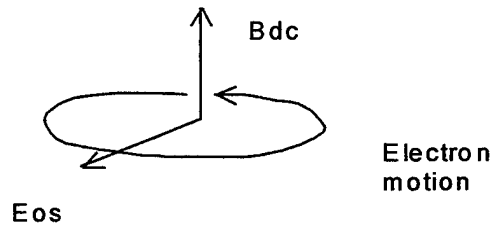


Figure 7. Cyclotron motion of an electron.

Large self-generated fields can significantly modify the interaction of the laser light with the plasma [Ref. 15]. This phenomenon can be explained by considering the oscillatory motion of the electrons, which results from the electric field of the incident laser light. The Lorentz force associated with this oscillation of electrons across the magnetic field is determined by :

$$\mathbf{F} = -e \mathbf{v}_{os} \times \mathbf{B}_{dc} . \quad (17)$$

In this equation, v_{os} is the velocity of electron oscillation in the laser field. This Lorentz force can become very strong. For $B_{dc} = 10^9$ Gauss and taking the peak $v_{os} = c$, the force corresponds to an oscillating electric field with amplitude of approximately 3×10^{11} V/cm! This large force can be expected to enhance the absorption efficiency, increase the heated electron energies, and lead to the generation of harmonics of the incident light. For a discussion of some of these effects at much lower intensities, see Ref. 16.

To demonstrate the effects of the self-generated fields, we used so called

1 1/2 D simulations (1 position, 2 velocities i.e. velocities in two directions for electrons and ions) with Zohar, a Particle-In-Cell code (PIC) that solves the complete set Maxwell's equations and uses relativistic dynamics [Ref. 7].

As shown in Figure 14, an intense light pulse was sent from vacuum onto a slab of overdense plasma.

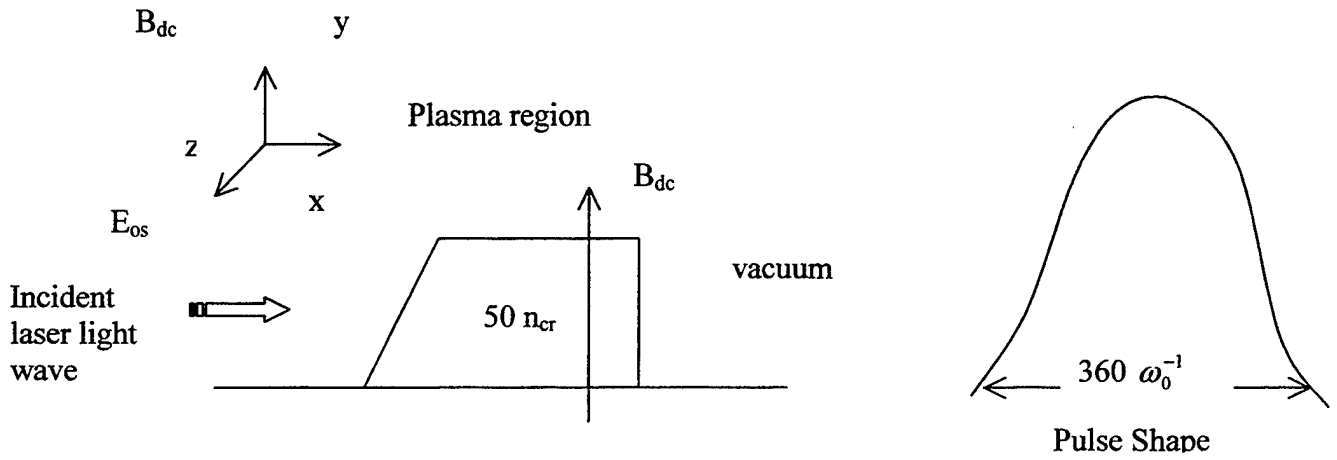
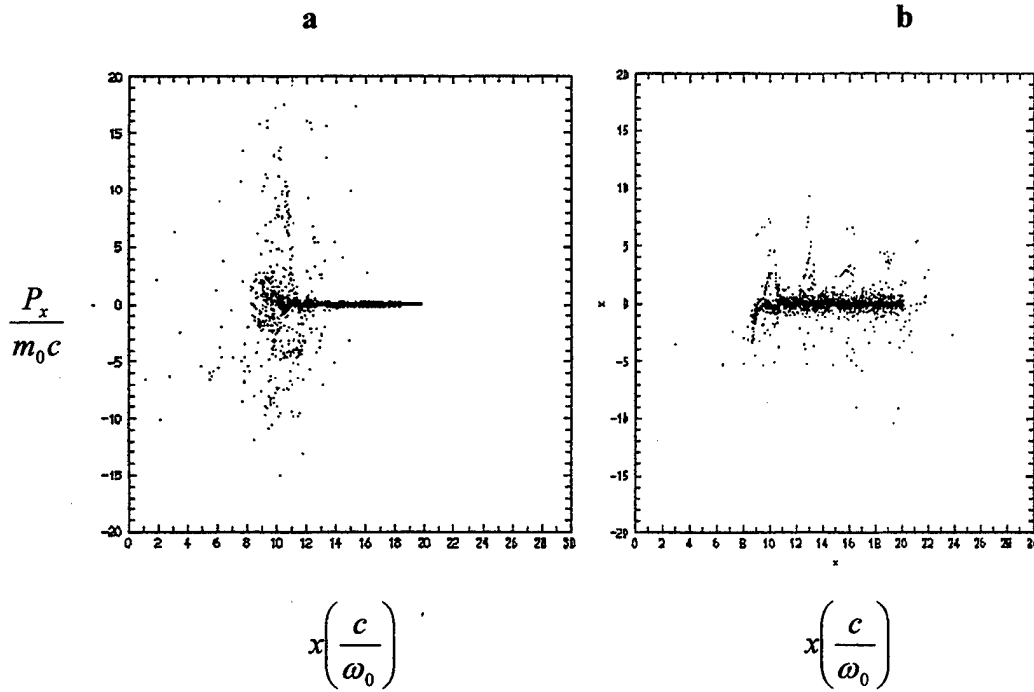


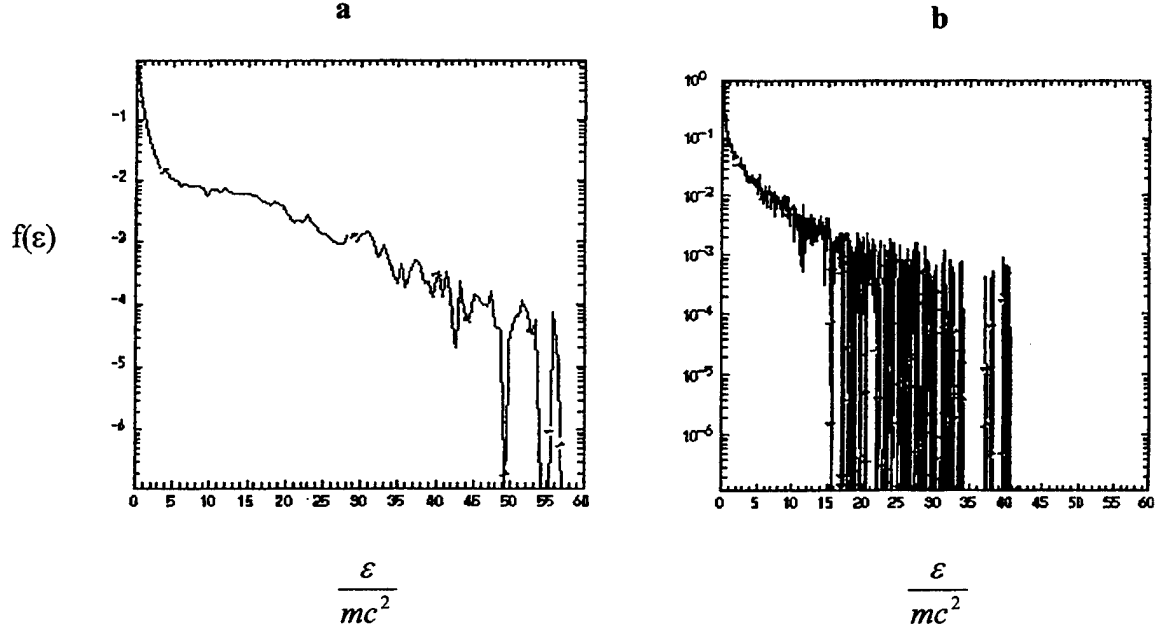
Figure 14. A schematic illustration of a computer simulation of intense laser light interacting with an overdense plasma.

In these simulations, a dc magnetic field pointing in the y direction was added in the code. The oscillating electric field of the laser light E_{os} was chosen to be either parallel or perpendicular to B_{dc} (by simply rotating the electric vector of the laser light 90°). Some typical parameters are shown in this figure. The initial plasma density rose rapidly to $50 \times n_{cr}$ where n_{cr} is the critical density. The intensity of incident light rose to its peak and then returned to zero in a time of $360 \omega_0^{-1}$. This corresponds to a pulse width of 180 fs (femtoseconds or 10^{-15} seconds) for $1.06 \mu\text{m}$ light.

To most simply illustrate the effects, consider an example in which the $1.06 \mu\text{m}$ laser light intensity is 10^{20} W/cm^2 , the magnitude of the imposed B_{dc} is 300 MG, and the ions are fixed. The enhanced heating due to the dc magnetic field is apparent in Figure (15), which shows electron phase space from simulations with and without the external B_{dc} field. More electrons are heated to higher velocity with the B field, as expected due to the additional force $(-e \mathbf{v}_{\text{os}} \times \mathbf{B}_{\text{dc}})$. Similar results can be seen from the distribution functions (number of electrons vs. energy) shown in Figure (16).



Figures 15 a,b. Snapshots of electron phase space in simulations a) with B_{dc} and b) without B_{dc} .



Figures 16 a, b. Plots showing numbers of electrons versus energy a) with B_{dc} field on b) without B_{dc} field.

Absorption can be measured by several different methods. In our approach, we chose to measure absorption by computing the change in kinetic energy of the plasma (from times before and after the laser pulse) and then dividing by the energy of the laser pulse. Figure 17 shows the absorbed energy versus time. In these simulations, the upper curve corresponds to the simulation with the magnetic field and the lower curve is the simulation without the magnetic field. If we normalize to the energy of the laser pulse, the fractional absorption was approximately 19% without B_{dc} ; it rose to about 30% with B_{dc} .

We also ran a simulation with B_{dc} , but with it pointing in the Z-direction. In this orientation v_{os} and B_{dc} are parallel, meaning that $v_{os} \times B_{dc} = 0$. As we expected, there was no enhancement of the absorption observed.

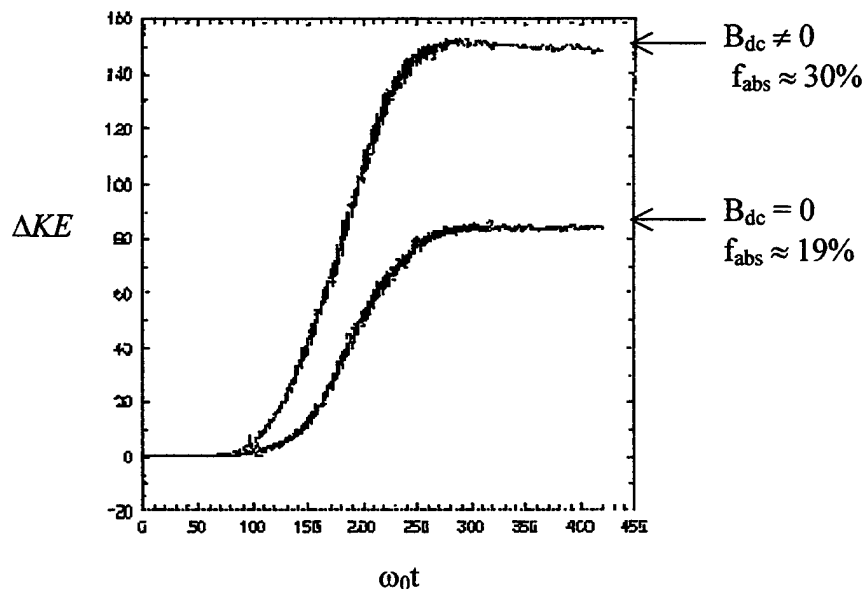


Figure 17 showing enhanced absorption when B_{dc} is turned on.

The simulations also show that the force due to oscillations of electrons across B_{dc} leads to an intense generation of even harmonics in the reflected light (see Figure 18). These even harmonics arise from the beating of the incident light wave with the density fluctuation driven by the $v_{os} \times B_{dc}$ force. In addition, there is enhanced radiation at lower frequency i.e. $\omega \leq \omega_{ce}$ which we attribute to radiation by electrons as they gyrate about the strong B_{dc} field. It would be interesting to look for this radiation in experiments, as detection of this radiation may serve as a diagnostic for the large self-generated fields that we propose can be generated in the ultra-intense laser regime.

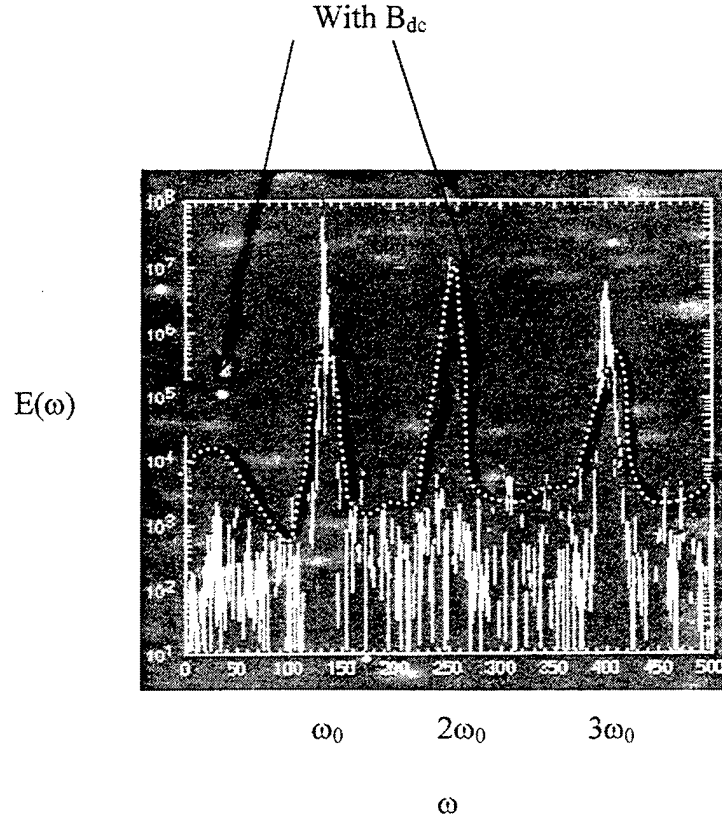


Figure 18. Frequency components of the reflected electric field showing even harmonics with B_{dc} .

Lastly, we carry out the same simulations allowing the ions to move. The electron-ion mass ratio is taken to be $1/3700$ (i.e. $m_e/m_i = 1/3700$). As shown in Figure 19, we again find that the absorption is greater with B_{dc} ($\approx 20\%$) than without B_{dc} ($f_{abs} \approx 2\%$). It is somewhat reduced in both cases because the intense pressure of the incident

light wave strongly steepened the density profile of the plasma. Again, we find that the heated electrons are significantly more energetic in the simulation with B_{dc} . This is clear from the electron phase spaces shown in Figure 20.

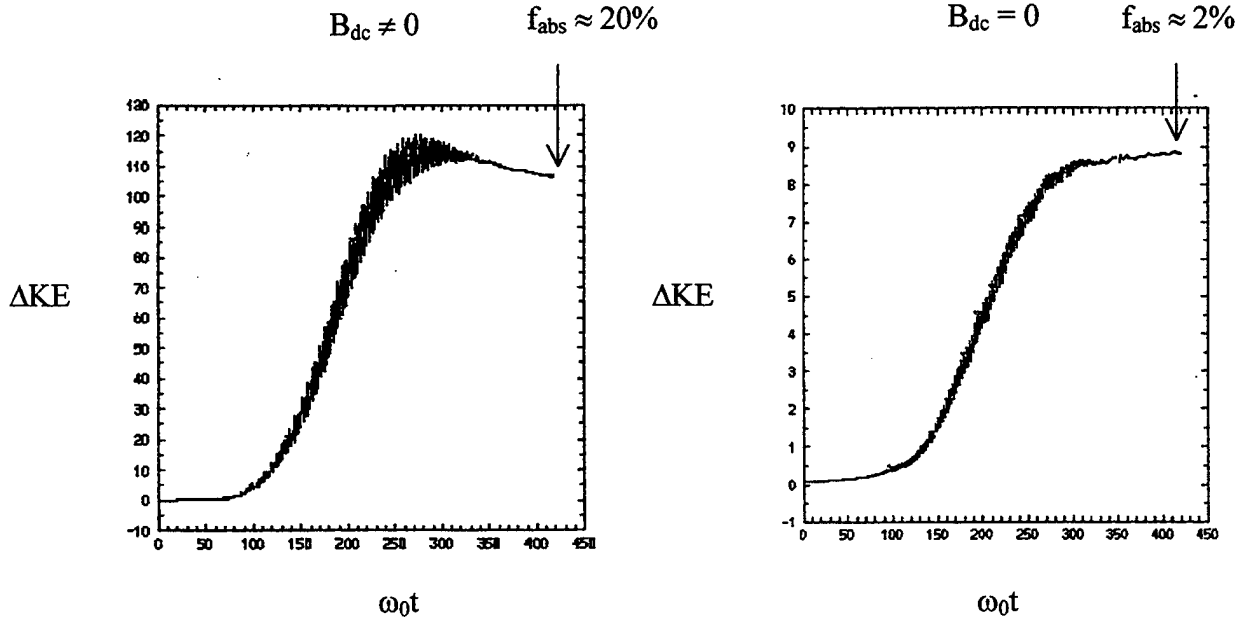


Figure 19. Plots showing enhanced absorption with B_{dc} .

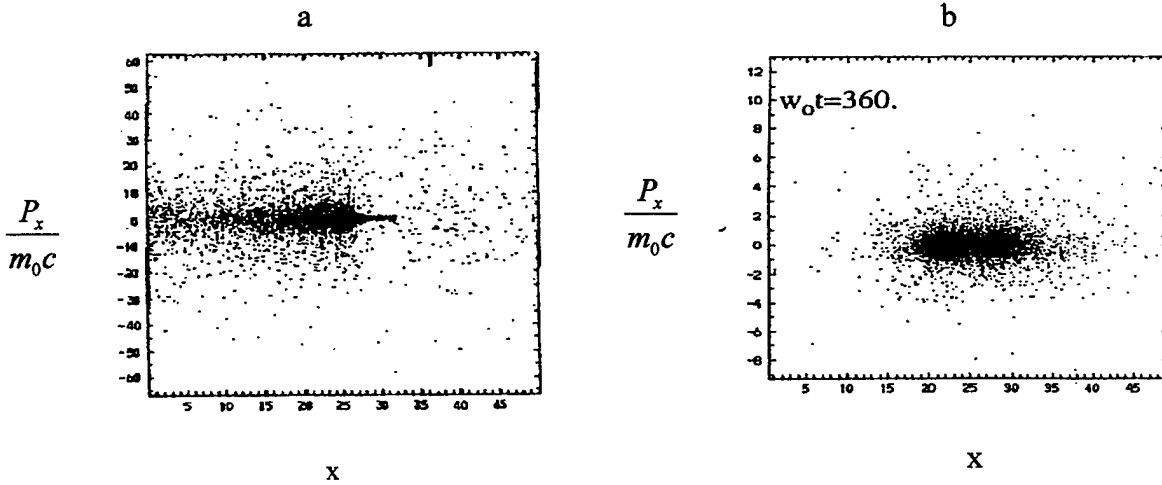


Figure 20. Plots of electron phase space in simulations with moving ions a) with and b) without B_{dc} .

The ion phase space shown in Figure 21 illustrates the ion acceleration into vacuum on both sides of the plasma. This acceleration is produced by the electric field that sets up to prevent the electrons from leaving the ions behind. Note also in Figure 21 the strong ion acceleration as the pressure of the intense light pushes on the plasma. With B_{dc} , ions that are more energetic are generated both in the expanding plasma and at the light-plasma interface.

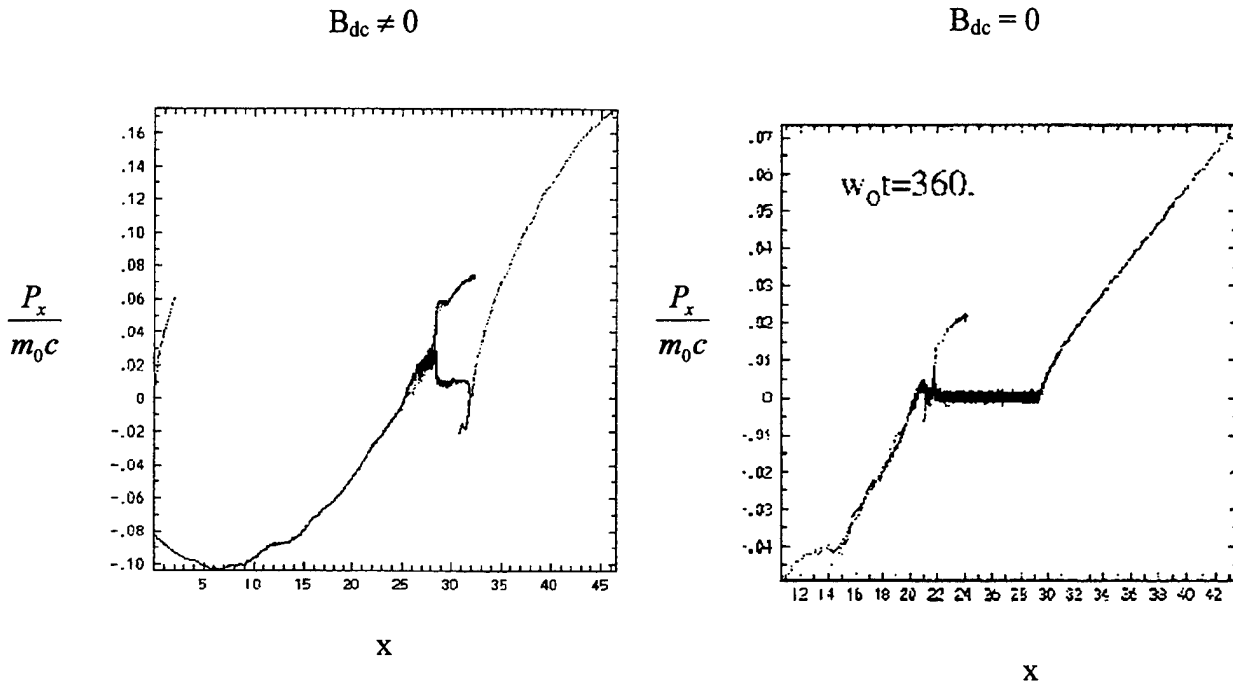


Figure 21. Simulations of Ion phase space with and without B_{dc}

Finally, the simulations show a very interesting compression of the B_{dc} . The pressure of the intense light wave compresses the density of the plasma, as it reflects (and partially absorbs). The peak magnitude of the field can be significantly increased. As seen in Figure 22, the peak B_{dc} has gone up by a factor of about three, which corresponds to over 10^9 Gauss in this particular example.

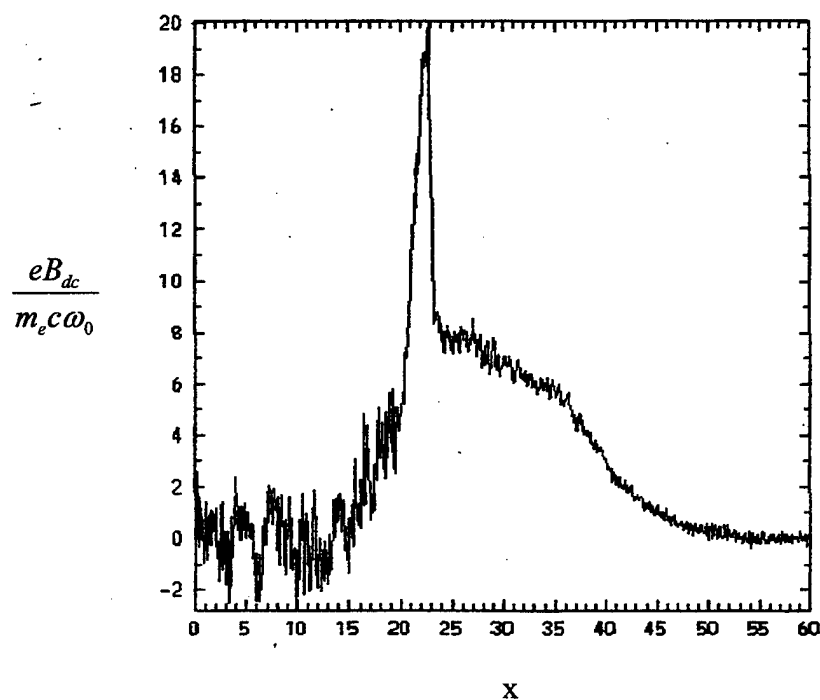


Figure 22. Simulation of the spatial profile of the magnitude of the self-generated magnetic field after irradiation by an intense laser pulse with intensity of 10^{21} W/cm².

THIS PAGE INTENTIONALLY LEFT BLANK

IV. CONCLUSION

We have investigated via computer simulations how self-generated magnetic fields up to 10^9 Gauss affect the interaction of short, ultra-intense pulses of laser light with plasmas. We have shown that the laser absorption and the high-energy electron generation can be significantly enhanced by these self-generated magnetic fields. The enhancement is attributed to the very large Lorentz forces resulting from the oscillation of electrons by the laser light across these fields.

Other effects shown are the generation of intense harmonics in the reflected light and noticeable cyclotron radiation. Finally, the large self-generated magnetic fields can be compressed to even large values by the pressure of the ultra-intense laser light.

Since the late 1970's, the existence of self-generated magnetic fields, in laser-irradiated targets, have been investigated. Some of the initial research confirming the existence of these magnetic fields was conducted by scientists at the Naval Research Lab [Ref. 17]. To attain magnetic fields on the order of 10^9 Gauss, which we have considered, requires a powerful laser capable of irradiating a target with intensities on the order of 10^{21} W/cm². Already, such intensities have been achieved by the "Petawatt", short pulse laser at the Lawrence Livermore National Laboratory.

Exciting high-energy applications and new research in creating Antimatter using ultra-intense lasers like Petawatt laser is being conducted. As an example, intense light from the Petawatt laser has been directed onto a thin gold film where it creates a plasma plume, which acts as a sort of messy Wakefield accelerator [Ref. 18] (see Figure 23). In particular, the electric field of the laser light rips electrons from the gold atoms and send the electrons shooting off with energies as high as 100 MeV.

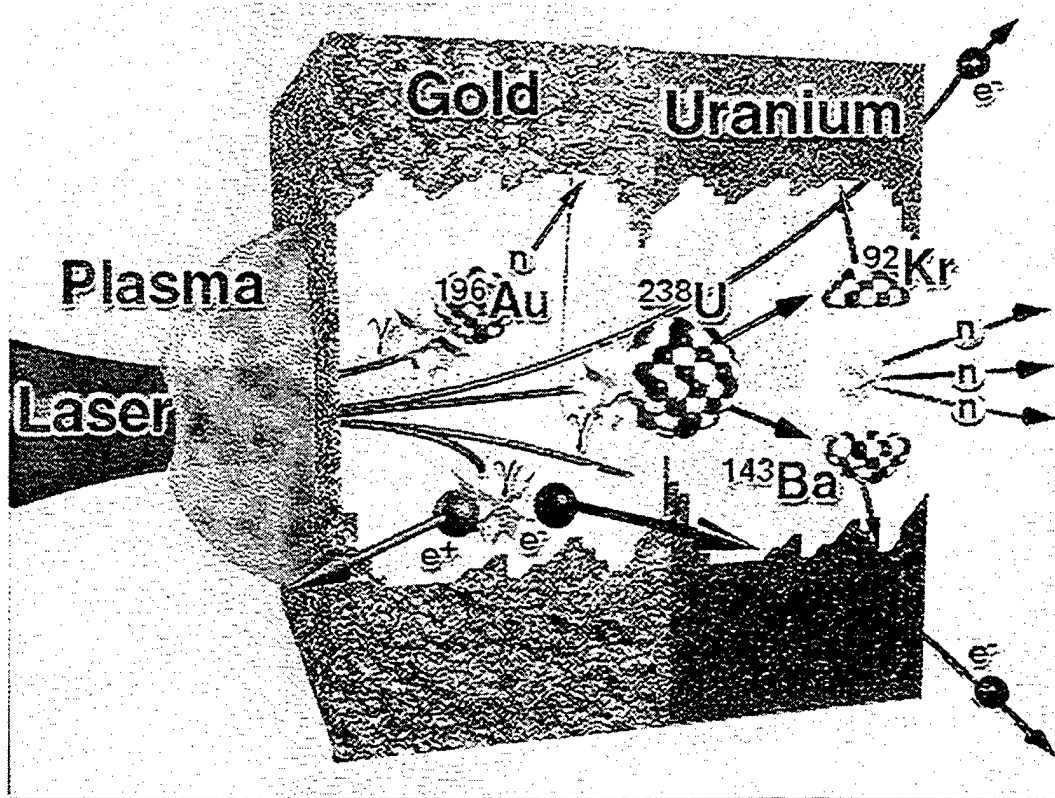


Figure 23. Illustration of an ultra-intense laser matter interaction. The laser's electric field is strong enough to rip electrons from the gold atoms and shoot them off with energies up to 100 MeV, initiating the generation of γ rays, which in turn can initiate fission or the generation of anti-matter (electron-positron pairs), From Ref.[18].

The generation of the relatively lower 3-10 MeV electrons using ultra-intense laser light (intensity about 10^{21} W/cm²), is an important issue for laser radiography. Some of the higher energy electrons radiate gamma rays, which in turn can induce fission or create electron-positron pairs (the first antimatter made in laser-solid interactions). A positron is an electron with a positive charge and is the anti-particle of the electron. The positron does not exist naturally on our planet. It 'arrives' in cosmic radiation or is created in the laboratory. Thus, laser photons at the electron-volt level can, by teaming up, initiate the sort of million-electron-volt nuclear reactions that normally take place only in an accelerator. Moreover, the femtoseconds laser pulses can be focused to a much smaller spot size than is possible with any conventional particle beam .

Continued enhancements and improvements in technology offer rich and exciting frontiers of science to be explored. Continued probing and exploring of the ultra-intense regime of laser plasma interactions shall give more understanding of very high temperature matter. This understanding will define and point to new applications, ranging from developments in laser radiography to the successful application of the fast ignition concept of inertial confinement fusion.

THIS PAGE INTENTIONALLY LEFT BLANK

LIST OF REFERENCES

1. Kruer, William L., *Physics of Laser Plasma Interactions*, (Addison-Wesley), Redwood City, 1988
2. Chen, Francis F., *Introduction to Plasma Physics and Controlled Fusion Vol I.* (Plenum Press), New York, NY, 1984
3. Stranger, J. A. et al., Phys. Rev. Letters 26, 1012 (1971)
4. Haines, M.G., Can. J. Phys. Rev. Letters 64, 912 (1986)
5. Birdsall, C. K., and Langdon, A. B., *Plasma Physics via Computer Simulation*, Institute of Physics Publishing, Philadelphia, PA, 1998
6. Denavit, J. and Kruer, William L., "How to get Started in Particle Simulation", Comments Plasma Physics and Controlled Fusion 6, 35 (1980). Also, Lawrence Livermore National Laboratory UCRL-84293 (1980)
7. Langdon, A. B. and Lasinski, B.F., "Methods in Computational Physics", edited by B. Adler, S. Fernback, M. Rotenberg and J. Killeen (Academic, New York, 1976) Volume 16, p. 327
8. A. Pukhov and J. Meyer-ter-Vehn, Phys. Rev. Letters 77, 3975 (1996)
9. H.X. Vu, J. Comput. Phys. 124, 417 (1996)
10. M.D. Perry and G. Mourou, Science 264m 917 (1994)
11. Wilks, Scott C. and Kruer, William L., IEEE Journal of Quantum Electronics, Vol. 33, NO. 11, November 1997 and many references therein
12. Tabak, M. et. al. Phys. Plasmas 1, 162 (1994)
13. Wilks, S. C., Kruer, W. L., Tabak, M and Langdon, A. B., Phys. Review Letters 69,1383 (1992)
14. Halliday, Resnick, and Walker, *Fundamentals of Physics-Extended, Fifth-Edition*, John Wiley and Sons, Inc., New York, NY, 1997
15. Tartt, Kent A, Wilks, S.C. and Kruer, W. L. paper 1P5, 30th Anomalous Absorption Conference, Ocean City, MD, May 21-26, 2000
16. Kruer, William L., and Estabrook, K. G., Phys. Fluids 20, 1688 (1977)

17. Gordon, D.F. Naval Research Lab, Oral Session 3O10, 30th Anomalous Absorption Conference, Ocean City, MD, 22 May 2000
18. Yaffa ad Shalom Eliezer, *The Fourth State of Matter*, IOP Publishing, Philadelphia, PA, 1989
19. Kruer, William L., "Plasma Simulations using Particle Codes", Nuclear Technology 27, 216 (1975)

INITIAL DISTRIBUTION

1. Defense Technical Information Center2
8725 John J. Kingman Rd., STE 0944
Ft. Belvoir, VA 22060-6218

2. Dudley Knox Library2
Naval Postgraduate School
441 Dyer Rd.
Monterey, CA 93943-5101

3. Engineering and Technology Curricular Office, Code 341
Naval Postgraduate School
Monterey, CA 93943

4. Professor William L. Kruer, Code PH/Kw1
Naval Postgraduate School
Monterey, CA 93943

5. Professor William B. Colson, Code PH/Cw1
Naval Postgraduate School
Monterey, CA 93943

6. Scott C. Wilks1
Lawrence Livermore National Labs
P.O. Box 808, L-039
Livermore, CA 94551

7. Kent A. Tartt1
784 Northridge PMB 273
Salinas, CA 93906-2015

8. Chairman, Department of Physics, Code PH.....2
Naval Postgraduate School
Monterey, CA 93943